DOI: 10.1002/cssc.201100525

# CO Oxidation at the Perimeters of an FeO/Pt(111) Interface and how Water Promotes the Activity: A First-Principles Study

Xiang-Kui Gu, Runhai Ouyang, Dapeng Sun, Hai-Yan Su, and Wei-Xue Li*[a]

The catalytic role of the Pt–Fe cation ensemble presented at the perimeters of the FeO film supported on Pt(111) for low-temperature CO oxidation and the promotion of water on activity were studied by using DFT calculations. We found that the perimeter sites along the edge of the FeO islands on Pt provided a favorable ensemble that consisted of coordinatively unsaturated ferrous species and nearby Pt atoms for $O_2$ and $H_2O$ activation free from CO poison. A dissociative oxygen atom at the Pt–Fe cation ensemble reacts easily with CO adsorbed on nearby Pt. The OH group from water dissociation not only facilitates activation of the oxygen molecule, more importantly it opens a facile reaction channel for CO oxidation through the formation of the carboxyl intermediate. The presence of the OH group on the FeO film strengthens interfacial interactions between FeO and Pt(111), which would make the FeO film more resistant to further oxidation. The importance of the Pt–Fe cation ensemble and the role of water as a cocatalyst for low-temperature CO oxidation is highlighted.

## Introduction

Proton exchange membrane fuel cells (PEMFCs) have attracted considerable attention, as they can efficiently convert chemical energy into electric energy through the reaction between $H_2$ and $O_2$ with water as the only product and no pollutant emission. For the anode reaction of the PEMFC, the utilized $H_2$ fuel mostly comes from steam reforming of various hydrocarbons.[1] The presence of CO byproduct at a concentration as low as 10 ppm would poison the Pt anode.[2] To afford purified hydrogen fuel for the PEMFC anode, the removal of CO from the reforming products under the operating conditions is required, but remains challenging. Among others, CO preferential oxidation (PROX) in excess $H_2$ at low temperatures has been considered to be promising and studied extensively.[3] So far, experimental and theoretical studies have been focused on more active and selective bimetallic Pt-based alloy catalysts, such as Pt/Ru,[3d] Pt/Co,[3g] Pt/Ni,[3h] and Pt/Fe.[4] Conversely, low-temperature CO oxidation, as a probe reaction to understand the structure–activity relationship of the catalysts, has also been investigated in depth on transition-metal (TM) surfaces,[5] inverse oxide films on TM surfaces,[6] and oxide-supported metal nanoparticles.[7]

Generally, the Langmuir–Hinshelwood mechanism applies for CO oxidation on TM surfaces, and the elementary reactions include mainly CO and $O_2$ adsorption, $O_2$ dissociation, and the reaction of CO with dissociative atomic O to form $CO_2$. Among these, $O_2$ dissociative adsorption at low temperatures is crucial and the rate-limiting step, in particular, for the late noble TM catalysts, such as Pt. When CO and $O_2$ competitively adsorb on Pt, the surface is dominated gradually by CO because of its stronger binding with Pt. As a consequence, a limited amount of sites are available for $O_2$ adsorption and activation, and the activity of CO oxidation is low. DFT calculations showed that $O_2$ dissociative adsorption on Pt(111) becomes endothermic when CO coverage is larger than 0.44 monolayers (MLs).[8] The development of bifunctional Pt-based catalysts free from CO poison at low temperatures is desired. For example, the addition of Fe on supported Pt catalysts dramatically increased the activity of CO oxidation and has been studied extensively.[4] Based on DFT calculations and surface science experiments on a FeO/Pt(111) model surface, we found recently that FeO/Pt(111) was highly active for $O_2$ activation and CO oxidation.[6c] The presence of the Pt–Fe cation ensemble, which consisted of a coordinatively unsaturated ferrous (CUF) species at the perimeters of the FeO nanoislands supported on Pt for $O_2$ activation and neighboring Pt atoms for CO adsorption, was essential.

In addition, water present in the reforming products and environment greatly affected low-temperature CO oxidation. For a Pt single crystal, Bergeld et al. observed that $CO_2$ formation was enhanced at approximately 200 K when $H_2O$ was added to the co-adsorbed CO and O on Pt(111).[9] DFT calculations on Pt(111) by Gong et al. revealed that the presence of water could stabilize the transition state (TS) of the reaction between CO and O by formation of hydrogen bonds.[10] Furthermore, the reaction of CO with OH groups at the perimeters of the FeO islands on Pt(111) was identified experimentally by Huang and coworkers.[11] For supported Pt catalysts, Fukuoka et al. found that CO oxidation was accelerated by the attack of OH on mesoporous $SiO_2$ to CO on Pt under PROX reaction conditions.[12] Tanaka et al. found that the oxidation of CO was mark-

[a] X.-K. Gu, R. Ouyang, D. Sun, Dr. H.-Y. Su, Prof. Dr. W.-X. Li
State Key Laboratory of Catalysis and Center for
Theoretical and Computational Chemistry
Dalian Institute of Chemical Physics
Chinese Academy of Sciences
Zhongshan Road 457, Dalian 116023 (P.R. China)
E-mail: wxli@dicp.ac.cn

  

edly enhanced by the presence of water for the PROX reaction on $FeO_x/Pt/TiO_2$ at 60 °C, and the measurement from in situ diffuse reflectance infrared Fourier transform (DRIFT) spectroscopy indicated that the enhancement mainly resulted from the involvement of OH groups in the reaction and formation of the HCOO intermediate.[4c,d] Promotion of water on low-temperature CO oxidation has also been found on Au catalysts.[13]

As indicated above, there are two possible roles for water promotion on CO oxidation, namely, indirectly by stabilizing the adsorption of reactants and/or the TS, or directly by forming the COOH intermediate. For both roles, the efficient adsorption and dissociation of water is a prerequisite. Water adsorption on the late TM surfaces is rather weak and falls typically in the range of −0.30 eV for water monomer adsorption,[14] while the dissociation barrier is considerable, for instance, 1.24 eV on Cu(111) and 1.01 eV on Pd(111).[15] This tells us that for late TM surfaces alone, the participation of water in the reaction would be limited and more sites available for water adsorption and activation would be required. It was reported that water activation could be facilitated at the metal/oxide interface.[16] However, the detailed mechanistic understanding of low-temperature CO oxidation in the presence of water on the metal/oxide catalysts remains unclear.

Aiming to shed light on the bifunctional role of the metal/oxide catalysts, we studied CO oxidation on the FeO/Pt(111) surface by using DFT calculations, and the result on Pt(111) was included for comparison. The Pt–Fe cation ensemble at the perimeters of the supported FeO islands for $O_2$ activation and neighboring Pt atoms for CO adsorption (free from site competition) was illustrated. Moreover, we found that the ensemble was reactive for water activation, and the OH formed oxidized easily with CO to $CO_2$ through the dehydrogenation of the COOH intermediate. The role of water as a cocatalyst is discussed.

## Computational Methods

Spin-polarized DFT calculations were performed by using the Vienna ab initio Simulation Package (VASP) based on the projected augmented wave (PAW) method.[17] The exchange-correlation interaction was described by using the generalized gradient approximation (GGA)[18] and the Perdew–Wang 91 (PW91) functional.[19] The Kohn–Sham equations were solved by using a plane-wave basis set with a kinetic energy cutoff of 400 eV. Because of the on-site Coulomb repulsion between d electrons, current exchange-correlation functionals fail to describe the electrons of transition metal (TM) oxides. To overcome this shortcoming, the DFT+U approach[20] was used to describe FeO with values of $U = 4$ eV and $J = 1$ eV for Fe 3d orbitals.

To model the reaction at the perimeters of the FeO film supported on Pt(111) and take into account the lattice mismatch between FeO and Pt(111), a slab model of a $(2\sqrt{3} \times 5)$ rectangular supercell was used, including three Pt(111) metal layers (20 Pt atoms in each layer) with the optimized Pt bulk lattice constant of 3.985 Å. The three-layer Pt slab was used to simulate the Pt substrate because the difference to that of seven layers was negligible.[21] On the Pt substrate, a bilayer FeO ribbon with three columns of Fe atoms (nine Fe atoms) and two columns of O atoms (six O atoms) was used to model the perimeters of the FeO nanoislands, as shown in Figure 1. The Fe atoms of the FeO ribbon coordinate with the topmost Pt layer at the interface. The average Fe–Fe distance in the ribbon is approximately 3.13 Å, which agrees well with the lattice parameter of 3.10 Å in the FeO/Pt(111) superstructure observed.[22]

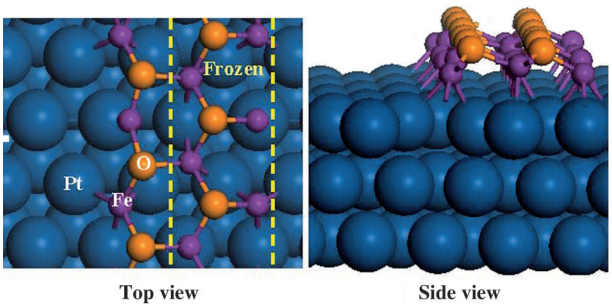


**Figure 1.** Structure of FeO/Pt(111). The Fe and O atoms in the yellow region were frozen during optimization. The blue, purple, and brown spheres represent Pt, Fe, and O atoms, respectively.

Two special $k$ points were used to sample the surface Brillouin zone integration of the $(2\sqrt{3} \times 5)$ FeO/Pt(111) slab. To prevent artificial interactions between the repeated slabs along the $z$ direction, a 12 Å vacuum was introduced with correction of the dipole moment. Adsorption was allowed on the side of the slab involving the FeO ribbon. During the optimization, the bottom two Pt layers and three right columns (two Fe columns and one O column, as indicated in Figure 1) were frozen, while the remaining atoms in the slab and adsorbates were relaxed until the residual forces were less than 0.05 eV Å$^{-1}$. The adsorption energies were calculated by using Equation (1):

$$E_{ads} = E_{ad/sub} - E_{ad} - E_{sub} \quad (1)$$

in which $E_{ad/sub}$, $E_{ad}$, and $E_{sub}$ were the total energies of the optimized adsorbate/substrate system, the adsorbate in the gas phase, and the clean substrate, respectively. The reaction energy ($E_r$) of the elementary step was calculated by using the total energy difference between products/substrate and reactants/substrate. Following convention, negative values of $E_{ads}$ and $E_r$ indicate an exothermic and energetically favorable process. The reaction barriers ($E_a$) and the transitional states (TSs) were searched by using the climbing-image nudged elastic band (CI-NEB) method.[23] All total energies were extrapolated to zero temperature without including a zero-point energy correction.

## Results and Discussion

In the perimeter region of the FeO ribbon on Pt(111), the exposed Fe cation at the FeO edge (CUF species) and nearby Pt form the so-called Pt–Fe cation ensemble, as indicated in Figure 1, which is key to the chemistry and will be explored herein.

### Adsorption of CO, $H_2O$, and $O_2$

The optimized structures and calculated adsorption energies for CO, $O_2$, and $H_2O$ on FeO/Pt(111) are shown in Figure 2. For comparison with a clean Pt surface, a Pt(111)-(2×2) slab was studied. The calculations show that CO tends to perpendicularly adsorb on the top of Pt (Figure 2a), giving significant ad-

  

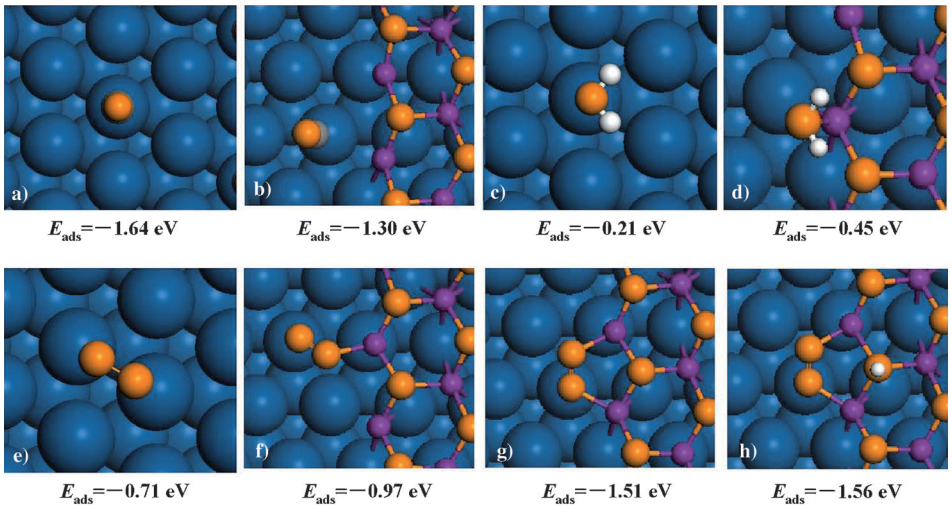


**Figure 2.** The optimized structures (top view) and calculated adsorption energies of the reactants on Pt(111) [a) CO, c) $H_2O$, and e) $O_2$] and FeO/Pt(111) [b) CO, d) $H_2O$, and f–h) $O_2$] with Pt–Fe cation ensemble. Pt, Fe, C, O, and H are represented by blue, purple, gray, brown, and white spheres, respectively.

sorption with an energy of −1.64 eV. When CO approaches the Pt–Fe cation ensemble in the perimeter region of the FeO/Pt(111), it becomes tilted backward from the normal direction by 13° (Figure 2b) to minimize steric repulsion between CO and FeO edge. The C–Pt bond length of the tilted CO is slightly longer (by 0.01 Å) than that of upright CO, and the calculated adsorption energy (−1.30 eV) becomes smaller. CO adsorption on the FeO(111) ribbon is endothermic. This agrees well with the experimental results, for which it was found that there was no CO adsorption on the Pt-supported FeO film.[24]

The adsorption and activation of $O_2$ are critical for low-temperature CO oxidation. On Pt(111), the most stable structure for $O_2$ adsorption is that in which the two oxygen atoms both bind to the adjacent top sites (Figure 2e). The O–O bond length is elongated to 1.38 Å, which is 0.14 Å longer than that in the gas phase. The calculated adsorption energy is −0.71 eV, much weaker than that of CO adsorption on Pt(111) (−1.64 eV) at a coverage of 0.25 ML. For $O_2$ adsorption at the Pt–Fe cation ensemble, it may coordinate either with one or two reactive CUF sites. For the first one (one O atom coordinated to one CUF site and the other to Pt, see Figure 2f), the calculated adsorption energy is −0.97 eV, which remains weaker than that of CO adsorption (−1.30 eV) in the same region. For the second one (Figure 2g), the calculated adsorption energy is −1.51 eV, which is stronger than that of CO adsorption. The Pt–Fe cation ensemble in the perimeter region of the FeO ribbon supported on Pt(111), therefore, provides new sites for $O_2$ adsorption free from CO poison. Herein, the optimized O–O bond length (1.43 Å) is 0.05 Å longer than that in the $O_2$/Pt(111) system, indicating that the $O_2$ molecule is more activated at the CUF sites along the perimeters. Finally, the presence of a lattice surface hydroxyl ($OH_L$) group near the edge of the FeO ribbon (as shown in Figure 2h) slightly enhances the $O_2$ adsorption with an energy of −1.56 eV.

Water monomer adsorbed on Pt(111) prefers to bind to the surface Pt through the O atom with a Pt–O distance of 2.47 Å (Figure 2c). The two O–H bonds are parallel to the surface. The interaction between water and Pt is weak with an adsorption energy of only −0.21 eV, which is consistent with the previous result of −0.27 eV.[25] Conversely, we found that water adsorption on the FeO ribbon was also very weak with an energy gain of −0.19 eV, which stems from the formation of the weak hydrogen bond between water and FeO. This is in line with the surface science findings of the chemical inertness of water on a pristine FeO film.[26] Alternatively, our calculations revealed that water adsorption at the Pt–Fe cation ensemble was stronger with an energy gain of −0.45 eV. Herein, water tends to bind to the CUF sites (see Figure 2d) through Fe–O($H_2$) bond formation with a bond length of 2.22 Å. This agrees well with recent STM experiments, in which water molecules were found to preferably stick to the edges of the FeO islands on Pt(111)[27] and Au(111).[28] If there is an O vacancy inside the FeO islands, water adsorption and dissociation could take place, as indicated in recent experiments.[29]

The above calculations show clearly that, compared to Pt(111), the Pt–Fe cation ensemble in the perimeter region of the FeO ribbon on Pt(111) provides active sites for $O_2$ and $H_2O$ adsorption free from CO poison. Moreover, the stronger binding of $H_2O$ at the ensemble also stabilizes water adsorption, which would facilitate its dissociation, as discussed below.

### Water dissociation

We now turn to water activation. As indicated before, water dissociation on late TM surfaces could be limited due to weak binding to the surfaces. This is particularly true when comparing the considerable dissociation barrier of 0.85 eV (similar to the previous calculation of 0.88 eV[25]) and endothermic reaction energy (0.61 eV) for 0.25 ML of water on Pt(111). The OH produced adsorbs at the top site with a binding energy of −2.29 eV (with respect to the OH radical in the gas phase). The O–Pt bond is 1.99 Å and the O–H bond is 73.55° tilted from the surface normal direction. The atomic H formed preferably adsorbs at the hollow site with a binding energy of −2.77 eV (with respect to atomic H in the gas phase). In addition, the water adsorption energy on Pt(111) is 1.43 eV smaller than that of CO adsorption. In other words, water adsorption and dissociation on Pt(111) would be blocked by CO. These results indicate clearly that, for low-temperature CO oxidation on Pt(111), the presence of water would barely affect the activity.

In contrast to Pt(111), water dissociation at the Pt–Fe cation ensemble is kinetically favorable. The calculated dissociation barrier is only 0.45 eV, as shown in Figure 3. The corresponding

  

reaction energy is slightly endothermic with a value of 0.08 eV, compared with that on the Pt(111) surface (0.61 eV). At the TS (Figure 3, TS), one of the two O–H bonds is elongated by 0.35 Å, and the abstract H atom approaches the lattice oxygen atom $O_L$ from the FeO edge to form $OH_L$ with a bond length of 0.97 Å. The binding energy of the abstract H with respect to $O_L$ is −2.68 eV, which is similar to that on Pt(111) (−2.77 eV). The left hydroxyl group of $H_2O$ (denoted $OH_F$) binds to the Pt–Fe cation ensemble with a Fe–O(H) bond length of 1.83 Å. The calculated binding energy of $OH_F$ is −2.98 eV, which is 0.69 eV stronger than that on Pt(111) (−2.29 eV). The stronger binding of the $OH_F$ at the Pt–Fe cation ensemble in the perimeter region greatly improves the reaction energy and also the kinetics. Taking enhanced water adsorption into account, these results clearly show that the Pt–Fe cation ensemble is highly active for water activation. This agrees well with recent experimental findings of low-temperature water activation and the formation of OH groups at the perimeters of FeO islands on Pt(111)[27] and Au(111).[28] The dissociation of water at the perimeter of $TiO_x$/Au(111) was studied previously by using DFT calculations,[16] and the modest barrier of approximately 0.60 eV obtained was in line with this study.

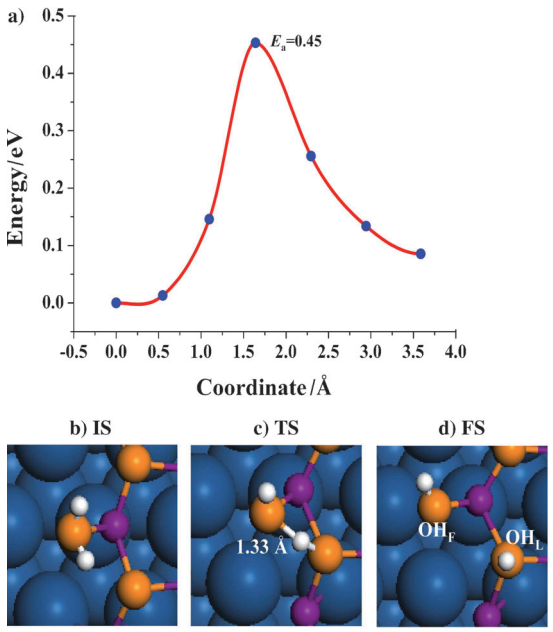


**Figure 3.** a) The potential energy surface of water dissociation at the Pt–Fe cation ensemble in the perimeter region of the FeO ribbon on the Pt(111) surface. The insets are the structures of the b) initial state (IS), c) the transitional state (TS), and d) the final state (FS), respectively.

### $O_2$ activation

The calculated potential energy surface for $O_2$ activation at the Pt–Fe cation ensemble is shown in Figure 4. Again, it was highly active with an $O_2$ dissociation barrier of 0.42 eV and a reaction energy of −0.68 eV. The length of O–O bond was elongated by 0.40 Å at the TS (Figure 4 TS1) with respect to the adsorbed state. After O–O bond breaking (Figure 4 FS1), the dissociative O atoms coordinated with two adjacent Fe cations and Pt atoms underneath. The dissociative adsorption energy is −1.10 eV per O atom with respect to $O_2$ in the gas phase. For O inside the FeO ribbon coordinated with three Fe cations, the dissociative adsorption energy is approximately −3.0 eV, which is too strong to be reactive. For dissociated oxygen at the Pt–Fe cation ensemble, one O–Fe bond is replaced by the relatively weak O–Pt bond, which makes dissociated $O_2$ more reactive.

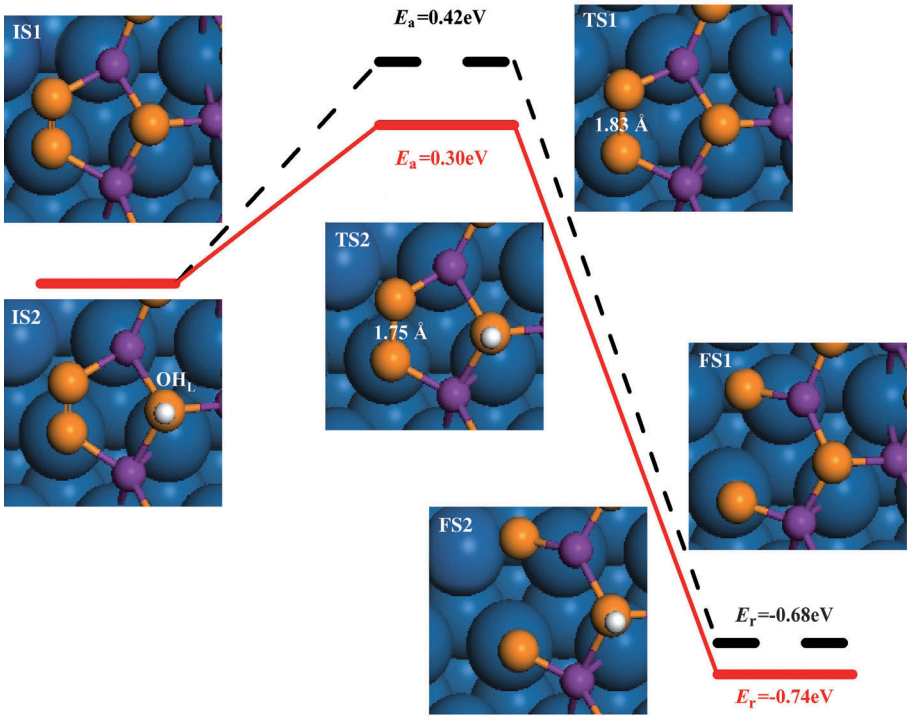


**Figure 4.** The activation barriers and reaction energies for $O_2$ dissociation at the Pt–Fe cation ensemble. The red solid and black dashed lines represent $O_2$ activation with and without the presence of the OH group, respectively. The insets are the structures (top view) of IS, TS, and FS for the reaction. IS1, TS1, and FS1 represent the results in the absence of the OH group, whereas IS2, TS2, and FS2 represent those in the presence of the OH group.

As mentioned above, the presence of $OH_L$ near the edge of the FeO ribbon stabilizes the adsorption of $O_2$ by 0.05 eV. We found that it could further facilitate $O_2$ dissociation. The calculated dissociation barrier in the presence of $OH_L$ was 0.30 eV, which was 0.12 eV lower than that in the absence of $OH_L$. The process released slightly more energy, 0.06 eV, and the dissociative adsorption energy was −1.13 eV per O atom. At the TS (Figure 4 TS2), the O–O bond was elongated further by 0.31 Å;

  

however, it remained 0.08 Å shorter than that in the absence of $OH_L$. In other words, the TS was approached earlier with less extension of the O–O bond in the presence of $OH_L$, and the corresponding barrier became lower. The reason might be attributable to the slight reduction of the CUF sites in the presence of $OH_L$. The calculated Bader charges of Fe cations along the FeO edge are $+1.16|e|$ and $+1.28|e|$ with and without the presence of $OH_L$, respectively. Further evidence can be found from the projected density of states (PDOS) at the TS (Figure 5): compared with the PDOS in the absence of the $OH_L$ group around the Fermi level, the Fe PDOS in the presence of the $OH_L$ group is shifted downward, and the electron population increases. Higher Fe metallicity leads to stronger binding with $O_2$ and stabilizes the TS, as expected.

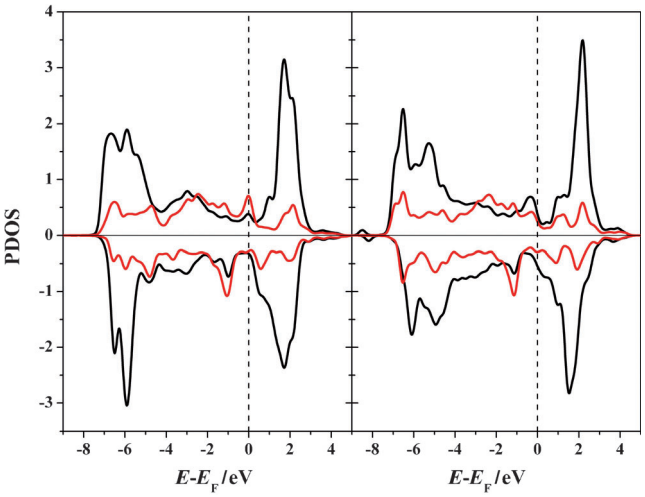


**Figure 5.** The PDOS of Fe 3d (black) and O 2p orbitals (red) at the TSs for $O_2$ activation. The right and left panels represent the results with and without the presence of $OH_L$, respectively.

## CO oxidation

Two types of reaction pathways for CO oxidation on FeO/Pt(111) were studied. For the first one, CO reacts with directly dissociated oxygen, and for the second one, CO reacts with OH from water dissociation. For comparison, we discuss briefly CO oxidation on a pure Pt(111) model catalyst; the calculated potential energy profile is shown in Figure 6. For $O_2$ dissociation on Pt(111), the barrier and reaction energies are 0.55 and −1.19 eV, respectively, and the TS is shown in Figure 6, TS1. For CO oxidation with dissociated oxygen (the TS plotted in Figure 6, TS2), the corresponding activation barrier and reaction energies are 0.85 and −0.57 eV, respectively. These values show that the elementary steps for CO oxidation on Pt(111), such as $O_2$ activation and the reaction of CO with atomic O on clean Pt(111), are not difficult. However, when CO and $O_2$ are exposed to Pt simultaneously, for example, at low temperature, the surface would be dominated by CO and $O_2$ dissociative adsorption is prevented.

The Pt–Fe cation ensemble provides active sites for $O_2$ and $H_2O$ adsorption and dissociation free from CO poison. The potential energy surfaces for the reaction of CO with dissociated oxygen and OH at the Pt–Fe cation ensemble are plotted in Figure 7. The calculated activation barrier and reaction energies for the reaction between CO and dissociated oxygen are 0.71 and −0.36 eV, respectively. During this reaction, CO adsorbed on Pt first diffuses toward the perimeter region and tilts backward to facilitate C–O bond formation. At the TS (Figure 7, TS1), the C–O bond formed is 1.87 Å long, which is 0.69 Å longer than that of $CO_2$ in the gas phase. However, the barrier reported in this study is slightly higher, by 0.08 eV, than our previously result of 0.63 eV.[6c] In that work, the CUF sites of the FeO ribbon were completely saturated with dissociated oxygen, and the stronger repulsive interaction between these O atoms led to them being more reactive. Once the $CO_2$ formed desorbed from the surface, the Pt–Fe cation ensemble was free for $O_2$ adsorption and activation, and thus, the catalytic cycle was closed. In this cycle, the rate-limiting step was the reaction between CO and atomic O with a barrier of 0.71 eV.

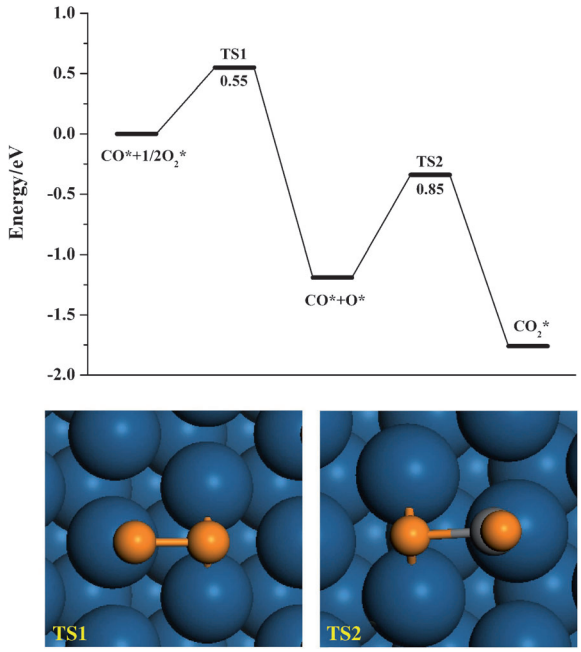


**Figure 6.** The potential energy profile for $O_2$ dissociation and reaction with CO on the Pt(111) surface. TS1 and TS2 are the structures of the TSs of $O_2$ dissociation and CO oxidation, respectively.

Compared with the reaction of CO directly with dissociated oxygen, the reaction of CO with $OH_F$ from water dissociation to form the carboxyl intermediate is kinetically more favorable. Although this step is endothermic by 0.16 eV, the activation barrier is only 0.33 eV, which is 0.38 eV lower than that of the reaction of CO directly with dissociated oxygen, as shown in Figure 7. This is in line with experiments conducted by Huang and coworkers,[11] who found that CO reacted easily with the interfacial OH at the boundary between the FeO island and supported Pt(111). To form the carboxyl intermediate, CO tilts backwards and binds to the O atom of $OH_F$. The distance between C and O is 1.89 Å at the TS (Figure 7, TS2), which is 0.44 Å longer than the bond in the carboxyl intermediate formed.

  

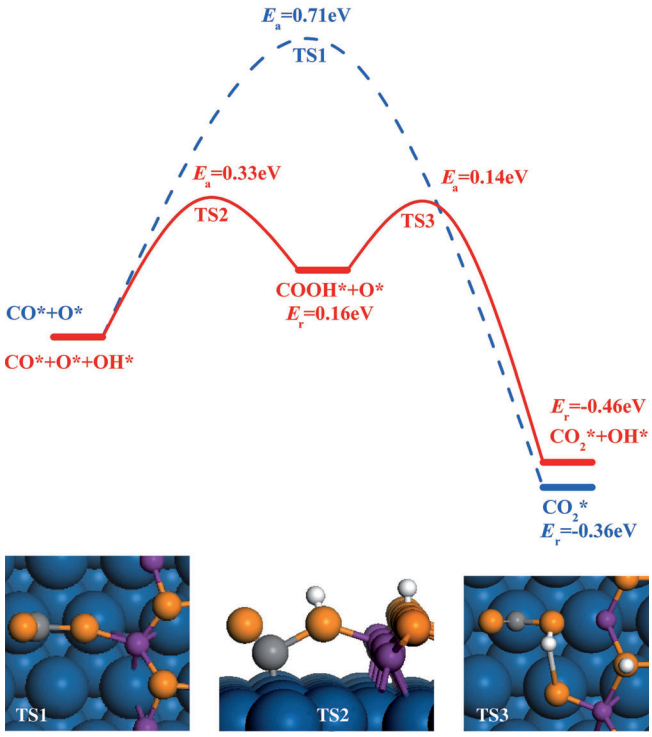


**Figure 7.** The potential energy surface and calculated activation barriers for the reaction of CO with dissociated oxygen (blue dashed line) and OH (red solid line) at the Pt–Fe cation ensemble. The insets of TS1, TS2, and TS3 are the TSs for the reaction of CO with dissociated oxygen and the reaction of CO with the OH group to form COOH and COOH dehydrogenation to products, respectively.

For $CO_2$ formation, the carboxyl intermediate formed could dehydrogenate to either dissociated oxygen or $OH_F$ at the Pt–Fe cation ensemble. We found that both reaction pathways were facile. The calculated barrier for the former was 0.14 eV with a reaction energy of −0.46 eV, forming $CO_2$ and $OH_F$, as indicated in Figure 7. The barrier for the latter one to form $CO_2$ and $H_2O$ was 0.17 eV with a reaction energy of −0.90 eV. The dehydrogenation of the carboxyl intermediate toward Pt is kinetically unfavorable. Gong et al. found that the corresponding barrier was 1.02 eV, which was much higher than those of the two reaction channels considered at the Pt–Fe cation ensemble.[10] For the two reaction channels considered herein, the byproducts formed are either $OH_F$ or $H_2O$. Both are the active species involved in the reaction and could participate again in subsequent reactions. In this cycle, the rate-limiting step is water dissociation with a barrier of only 0.45 eV (Figure 3), which is much lower than that of the reaction of CO directly with atomic O (0.71 eV).

The results so far show that water is involved in the reaction and promotes the activity of CO oxidation. Because the OH group and/or water are regenerated during the reaction, there is no consumption of the OH group and/or water in the whole catalytic cycle. In other words, water acts as a cocatalyst for CO oxidation on the FeO/Pt surface studied. This has been proposed in the past for CO oxidation on Au(111).[13f] In that work, to activate the water, Au(111) was precovered with atomic O; this is unlikely to occur under realistic conditions. On FeO/Pt(111), water adsorption and activation could be easily achieved at the Pt–Fe cation ensemble because of its strong binding with water molecules. The efficient activation of water at the metal cation ensemble was also found in the water-gas shift reaction at the perimeters of the inverse $CeO_x$/Au(111) and $TiO_x$/Au(111) model catalysts.[16] The scenario described, namely, the metal cation ensemble as the active site hosts in the perimeters of the metal oxide interface, which was also highly active for CO oxidation on the inverse $PtO_2$/Pt(111)-[30] and $TiO_2$-supported nano-Au catalysts,[31] should apply, in general, to various catalytic reactions and metal/oxide catalysts.

## OH-promoted interfacial interactions between FeO and Pt(111)

The high activity and flexibility of the Pt–Fe cation ensemble comes from the simultaneous exposure of distinct sites (metallic Pt and low-valent Fe cations) in a constrained space. The absence of either of them would lead to lower activity. For example, if the Pt substrate is completely covered by a FeO film and there is no Pt and low-valent Fe cation exposed, the activity is low.[32] Conversely, if the Fe valent state is rather high, its activity, for example, in $O_2$ activation, would also be limited. Previous experiments showed that under higher $O_2$ partial pressures, FeO films supported on Pt(111) was oxidized further to the trilayer structure (O–Fe–O).[6a,b] Correspondingly, the activity for CO oxidation became pronounced only at temperatures higher than 430 K. This is contrast to the room-temperature activity observed on FeO/Pt(111),[6c] for which the lower valent Fe cations exposed at the edge of the dispersed FeO islands are available. To maintain the activity of FeO islands, it is desirable to stabilize the supported FeO islands, which makes it more resistant to complete oxidation.

In this context, we note that the formation of a bilayer of FeO on Pt(111) comes from the strong interface interaction. This can be deduced from the calculated interfacial adhesion energy of −1.40 eV per FeO between FeO and Pt(111).[6c] It is expected that enhanced interfacial adhesion between FeO and Pt(111) would stabilize the FeO film and make it more resistant to complete oxidation. Interestingly, we found that interfacial adhesion between FeO and Pt(111) could be enhanced dramatically by the presence of OH groups on the FeO film. To illustrate this, we considered an epitaxial FeO/Pt(111)-(3×3) surface by assuming a Pt(111) lattice constant. The calculated interfacial adhesion energy in the absence of the OH group is −1.53 eV per FeO. The difference from our previous calculations[6c] comes from the different supercell used. If there is coverage of a 1/3 ML of OH on FeO/Pt(111)-(3×3), the calculated interfacial adhesion energy becomes −2.00 eV/FeO, and the interfacial interaction between FeO and Pt(111) becomes stronger. The interfacial interaction becomes even stronger with a further increase in OH coverage, as plotted in Figure 8 and summarized in Table 1. The underlying mechanism is rather straightforward. In the presence of the OH group, the interaction between Fe and the oxygen overlayer is weakened. As compensation, the interaction between Fe and Pt is enhanced,

  

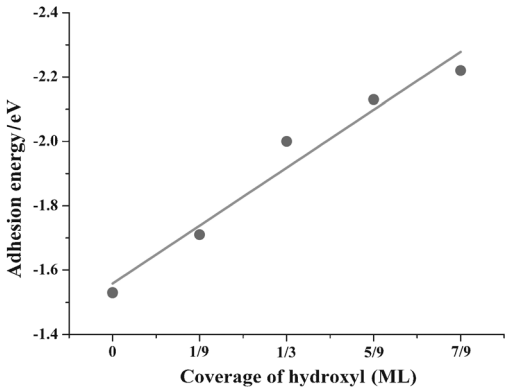


**Figure 8.** The variation of interfacial adhesion energy per FeO between FeO and Pt(111) with respect to the coverage of OH on FeO film.

**Table 1.** Interfacial adhesion energies (eV) between FeO and Pt associated with the coverage of the hydroxyl group in monolayers (ML).

| Coverage with ML | Adhesion energy [eV] |
|---|---|
| 0 | -1.53 |
| 1/9 | -1.71 |
| 1/3 | -2.00 |
| 5/9 | -2.13 |
| 7/9 | -2.22 |

as seen from the increase of electron accumulation at the Pt–Fe interface (not shown herein). The enhanced interfacial interaction between FeO and Pt(111) by the OH group would make FeO more resistant to the complete oxidation and maintain the stability of the Pt–Fe cation ensemble.

## Conclusions

Low-temperature CO oxidation on the inverse FeO/Pt(111) model surface, as well as the promotion of water on the activity, were investigated by using DFT calculations. We found that the presence of the Pt–Fe cation ensemble hosted in the perimeter region of the FeO islands on Pt(111) played a critical role for the low-temperature reactivity. The Pt–Fe cation ensemble was highly active for $O_2$ and $H_2O$ activation free from CO poison. The dissociative $O_2$ at the ensemble reacted easily with CO adsorbed on nearby Pt. The OH group formed through water dissociation at the Pt–Fe cation ensemble opened a new facile reaction channel for CO oxidation through the formation of the carboxyl intermediate, which was more reactive than that of CO oxidation with dissociated oxygen at the same site. During the reaction, water participates in the reaction as a cocatalyst without being consumed. Moreover, we found that the interfacial interaction between FeO and Pt could be enhanced greatly by the presence of OH groups, which prevented the complete oxidation of active low-valent Fe in the Pt–Fe cation ensemble. The unique activity and flexibility of the active-site metal cation ensemble stems from the simultaneous exposure of the distinct sites (metallic Pt and low-valent Fe cation) in a constrained space. Further studies of metal-cation ensembles in supported metal catalysts with improved activity and selectivity are worth exploring in the future.

## Acknowledgements

*We acknowledge financial support from the Natural Science Foundation of China (20733008 and 21173210). We appreciate fruitful discussions with Prof. Xinhe Bao and Qiang Fu.*

**Keywords:** iron · oxidation · platinum · surface chemistry · supported catalysts

[1] R. M. Navarro, M. A. Pena, J. L. G. Fierro, *Chem. Rev.* **2007**, *107*, 3952.
[2] G. J. K. Acres, J. C. Frost, G. A. Hards, R. J. Potter, T. R. Ralph, D. Thompsett, G. T. Burstein, G. J. Hutchings, *Catal. Today* **1997**, *38*, 393.
[3] a) I. H. Son, M. Shamsuzzoha, A. M. Lane, *J. Catal.* **2002**, *210*, 460; b) O. Pozdnyakova, D. Teschner, A. Wootsch, J. Krohnert, B. Steinhauer, H. Sauer, L. Toth, F. C. Jentoft, A. Knop-Gericke, Z. Paal, R. Schlögl, *J. Catal.* **2006**, *237*, 1; c) O. Pozdnyakova, D. Teschner, A. Wootsch, J. Krohnert, B. Steinhauer, H. Sauer, L. Toth, F. C. Jentoft, A. Knop-Gericke, Z. Paal, R. Schlögl, *J. Catal.* **2006**, *237*, 17; d) S. Alayoglu, A. U. Nilekar, M. Mavrikakis, B. Eichhorn, *Nat. Mater.* **2008**, *7*, 333; e) A. U. Nilekar, S. Alayoglu, B. Eichhorn, M. Mavrikakis, *J. Am. Chem. Soc.* **2010**, *132*, 7418; f) E. D. Park, D. Lee, H. C. Lee, *Catal. Today* **2009**, *139*, 280; g) D. J. Suh, C. Kwak, J. H. Kim, S. M. Kwon, T. J. Park, *J. Power Sources* **2005**, *142*, 70; h) H. Y. Su, X. H. Bao, W. X. Li, *J. Chem. Phys.* **2008**, *128*, 194707.
[4] a) A. Siani, B. Captain, O. S. Alexeev, E. Stafyla, A. B. Hungria, P. A. Midgley, J. M. Thomas, R. D. Adams, M. D. Amiridis, *Langmuir* **2006**, *22*, 5160; b) J. Yin, J. H. Wang, T. Zhang, X. D. Wang, *Catal. Lett.* **2008**, *125*, 76; c) K. Tanaka, M. Shou, H. He, X. Y. Shi, *Catal. Lett.* **2006**, *110*, 185; d) K. Tanaka, M. Shou, H. He, X. Y. Shi, X. L. Zhang, *J. Phys. Chem. C* **2009**, *113*, 12427.
[5] a) J. Z. Xu, J. T. Yates, *J. Chem. Phys.* **1993**, *99*, 725; b) G. Ertl, *Surf. Sci.* **1994**, *299*, 742; c) C. Stampfl, M. Scheffler, *Phys. Rev. Lett.* **1997**, *78*, 1500; d) Y. K. Kim, G. A. Morgan, J. T. Yates, *J. Phys. Chem. C* **2007**, *111*, 3366; e) J. Knudsen, L. R. Merte, G. W. Peng, R. T. Vang, A. Resta, E. Laegsgaard, J. N. Andersen, M. Mavrikakis, F. Besenbacher, *ACS Nano* **2010**, *4*, 4380; f) H. Y. Su, Z. H. Zeng, X. H. Bao, W. X. Li, *J. Phys. Chem. C* **2009**, *113*, 8266; g) H. Y. Su, X. K. Gu, X. F. Ma, Y. H. Zhao, X. H. Bao, W. X. Li, *Catal. Today* **2011**, *165*, 89.
[6] a) Y. N. Sun, Z. H. Qin, M. Lewandowski, E. Carrasco, M. Sterrer, S. Shaikhutdinov, H. J. Freund, *J. Catal.* **2009**, *266*, 359; b) Y. N. Sun, L. Giordano, J. Goniakowski, M. Lewandowski, Z. H. Qin, C. Noguera, S. Shaikhutdinov, G. Pacchioni, H. J. Freund, *Angew. Chem.* **2010**, *122*, 4520; *Angew. Chem. Int. Ed.* **2010**, *49*, 4418; c) Q. Fu, W. X. Li, Y. X. Yao, H. Y. Liu, H. Y. Su, D. Ma, X. K. Gu, L. M. Chen, Z. Wang, H. Zhang, B. Wang, X. H. Bao, *Science* **2010**, *328*, 1141; d) R. T. Mu, Q. Fu, H. Xu, H. Zhang, Y. Y. Huang, Z. Jiang, S. Zhang, D. L. Tan, X. H. Bao, *J. Am. Chem. Soc.* **2011**, *133*, 1978.
[7] a) M. Haruta, S. Tsubota, T. Kobayashi, H. Kageyama, M. J. Genet, B. Delmon, *J. Catal.* **1993**, *144*, 175; b) W. E. Kaden, W. A. Kunkel, M. D. Kane, F. S. Roberts, S. L. Anderson, *J. Am. Chem. Soc.* **2010**, *132*, 13097; c) Y. Liu, C. J. Jia, J. Yamasaki, O. Terasaki, F. Schüth, *Angew. Chem.* **2010**, *122*, 5907; *Angew. Chem. Int. Ed.* **2010**, *49*, 5771; d) Q. L. Li, Y. H. Zhang, G. X. Chen, J. Q. Fan, H. Q. Lan, Y. Q. Yang, *J. Catal.* **2010**, *273*, 167; e) S. A. C. Carabineiro, B. F. Machado, R. R. Bacsa, P. Serp, G. Drazic, J. L. Faria, J. L. Figueiredo, *J. Catal.* **2010**, *273*, 191.
[8] B. Shan, N. Kapur, J. Hyun, L. Wang, J. B. Nicholas, K. Cho, *J. Phys. Chem. C* **2009**, *113*, 710.
[9] J. Bergeld, B. Kasemo, D. V. Chakarov, *Surf. Sci.* **2001**, *495*, L815.
[10] X. Q. Gong, P. Hu, R. Raval, *J. Chem. Phys.* **2003**, *119*, 6324.
[11] L. S. Xu, Y. S. Ma, Y. L. Zhang, Z. Q. Jiang, W. X. Huang, *J. Am. Chem. Soc.* **2009**, *131*, 16366.
[12] A. Fukuoka, J. I. Kimura, T. Oshio, Y. Sakamoto, M. Ichikawa, *J. Am. Chem. Soc.* **2007**, *129*, 10120.
[13] a) M. Date, M. Haruta, *J. Catal.* **2001**, *201*, 221; b) M. Daté, M. Okumura, S. Tsubota, M. Haruta, *Angew. Chem.* **2004**, *116*, 2181; *Angew. Chem. Int.*

  

*Ed.* **2004**, *43*, 2129; c) C. K. Costello, M. C. Kung, H. S. Oh, Y. Wang, H. H. Kung, *Appl. Catal. A: Gen.* **2002**, *232*, 159; d) C. K. Costello, J. H. Yang, H. Y. Law, Y. Wang, J. N. Lin, L. D. Marks, M. C. Kung, H. H. Kung, *Appl. Catal. A: Gen.* **2003**, *243*, 15; e) M. C. Kung, R. J. Davis, H. H. Kung, *J. Phys. Chem. C* **2007**, *111*, 11767; f) R. A. Ojifinni, N. S. Froemming, J. Gong, M. Pan, T. S. Kim, J. M. White, G. Henkelman, C. B. Mullins, *J. Am. Chem. Soc.* **2008**, *130*, 6801; g) M. A. Debeila, R. P. K. Wells, J. A. Anderson, *J. Catal.* **2006**, *239*, 162; h) K. Qian, W. H. Zhang, H. X. Sun, J. Fang, B. He, Y. S. Ma, Z. Q. Jiang, S. Q. Wei, J. L. Yang, W. X. Huang, *J. Catal.* **2011**, *277*, 95; i) C. Shang, Z. P. Liu, *J. Phys. Chem. C* **2010**, *114*, 16989; j) L. M. Liu, B. McAllister, H. Q. Ye, P. Hu, *J. Am. Chem. Soc.* **2006**, *128*, 4017; k) H. Y. Su, M. M. Yang, X. H. Bao, W. X. Li, *J. Phys. Chem. C* **2008**, *112*, 17303.

[14] J. Carrasco, A. Michaelides, M. Scheffler, *J. Chem. Phys.* **2009**, *130*, 184707.

[15] X. K. Gu, W. X. Li, *J. Phys. Chem. C* **2010**, *114*, 21539.

[16] J. A. Rodriguez, S. Ma, P. Liu, J. Hrbek, J. Evans, M. Perez, *Science* **2007**, *318*, 1757.

[17] a) G. Kresse, J. Furthmuller, *Phys. Rev. B* **1996**, *54*, 11169; b) G. Kresse, J. Furthmuller, *Comput. Mater. Sci.* **1996**, *6*, 15.

[18] J. P. Perdew, K. Burke, M. Ernzerhof, *Phys. Rev. Lett.* **1996**, *77*, 3865.

[19] J. P. Perdew, Y. Wang, *Phys. Rev. B* **1992**, *45*, 13244.

[20] a) S. L. Dudarev, G. A. Botton, S. Y. Savrasov, C. J. Humphreys, A. P. Sutton, *Phys. Rev. B* **1998**, *57*, 1505; b) L. Giordano, G. Pacchioni, J. Goniakowski, N. Nilius, E. D. L. Rienks, H. J. Freund, *Phys. Rev. B* **2007**, *76*, 075416; c) R. Ouyang, W. X. Li, *Phys. Rev. B* **2011**, *84*, 165403.

[21] W. H. Zhang, Z. Y. Li, Y. Luo, J. L. Yang, *J. Phys. Chem. C* **2009**, *113*, 8302.

[22] a) Y. J. Kim, C. Westphal, R. X. Ynzunza, H. C. Galloway, M. Salmeron, M. A. VanHove, C. S. Fadley, *Phys. Rev. B* **1997**, *55*, R13448; b) Y. X. Yao, Q. Fu, Z. Wang, D. L. Tan, X. H. Bao, *J. Phys. Chem. C* **2010**, *114*, 17069.

[23] a) G. Henkelman, B. P. Uberuaga, H. Jonsson, *J. Chem. Phys.* **2000**, *113*, 9901; b) G. Henkelman, H. Jonsson, *J. Chem. Phys.* **2000**, *113*, 9978.

[24] C. Lemire, R. Meyer, V. E. Henrich, S. Shaikhutdinov, H. J. Freund, *Surf. Sci.* **2004**, *572*, 103.

[25] L. C. Grabow, A. A. Gokhale, S. T. Evans, J. A. Dumesic, M. Mavrikakis, *J. Phys. Chem. C* **2008**, *112*, 4608.

[26] a) Y. Joseph, W. Ranke, W. Weiss, *J. Phys. Chem. B* **2000**, *104*, 3224; b) W. Weiss, W. Ranke, *Prog. Surf. Sci.* **2002**, *70*, 1; c) U. Leist, W. Ranke, K. Al-Shamery, *Phys. Chem. Chem. Phys.* **2003**, *5*, 2435.

[27] W. Wang, H. Zhang, W. H. Wang, A. D. Zhao, B. Wang, J. G. Hou, *Chem. Phys. Lett.* **2010**, *500*, 76.

[28] X. Y. Deng, J. Lee, C. J. Wang, C. Matranga, F. Aksoy, Z. Liu, *Langmuir* **2011**, *27*, 2146.

[29] J. Knudsen, L. R. Merte, L. C. Grabow, F. M. Eichhorn, S. Porsgaard, H. Zeuthen, R. T. Vang, E. Laegsgaard, M. Mavrikakis, F. Besenbacher, *Surf. Sci.* **2010**, *604*, 11.

[30] W. X. Li, B. Hammer, *Chem. Phys. Lett.* **2005**, *409*, 1.

[31] I. X. Green, W. J. Tang, M. Neurock, J. T. Yates, *Science* **2011**, *333*, 736.

[32] a) W. X. Huang, W. Ranke, *Surf. Sci.* **2006**, *600*, 793; b) L. R. Merte, J. Knudsen, L. C. Grabow, R. T. Vang, E. Laegsgaard, M. Mavrikakis, F. Besenbacher, *Surf. Sci.* **2009**, *603*, L15.

Received: August 31, 2011
Revised: October 25, 2011
Published online on December 9, 2011

  